How dirt cones form on glaciers: Field observation, laboratory experiments, and modeling

Marceau Hénot [1,2] Vincent J. Langlois [3] Nicolas Plihon [1] and Nicolas Taberlet [1,*]

[1] *Université Lyon, ENS de Lyon, Université Claude Bernard, CNRS, Laboratoire de Physique, F-69342 Lyon, France*

[2] *SPEC, CEA, CNRS, Université Paris-Saclay, CEA Saclay Bat 772, 91191 Gif-sur-Yvette Cedex, France*

[3] *Laboratoire de Géologie de Lyon, Terre, Planètes, Environnement, Université Claude Bernard Lyon 1–ENS de Lyon–Université Jean Monnet Saint-Étienne–CNRS, France*

(Received 19 December 2022; accepted 13 March 2023; published 28 March 2023)

Dirt cones are meter-scale structures encountered at the surface of glaciers, which consist of ice cones covered by a thin layer of ashes, sand, or gravel, and which form naturally from an initial patch of debris. In this article, we report field observations of cone formation in the French Alps, laboratory-scale experiments reproducing these structures in a controlled environment, and two-dimensional discrete-element-method–finite-element-method numerical simulations coupling the grain mechanics and thermal effects. We show that cone formation originates from the insulating properties of the granular layer, which reduces ice melting underneath as compared to bare ice melting. This differential ablation deforms the ice surface and induces a quasistatic flow of grains that leads to a conic shape, as the thermal length become small compared to the structure size. The cone grows until it reaches a steady state in which the insulation provided by the dirt layer exactly compensates for the heat flux coming from the increased external surface of the structure. These results allowed us to identify the key physical mechanisms at play and to develop a model able to quantitatively reproduce the various field observations and experimental findings.

DOI: 10.1103/PhysRevE.107.034905

I. INTRODUCTION

Differential ablation of ice or snow (a disparity in the melting or sublimation rate) is a powerful driving force governing the formation of various natural structures. The mechanism of ablation can be sublimation in the case of blue ice ripples observed in Antarctica [1], elongated snow structures called penitentes found in the Andes mountains [2–4], or zen stones observed on Lake Baikal which consist of a pebble sitting on a centimetric ice foot caused by an umbrella effect [5]. Ice melting patterns are observed in various situations: scallops appear at the interface with water under the effect of turbulent flow [6,7], while suncups form on snow surfaces exposed to solar radiation [8,9]. For the latter, the presence of grains in the snow can play a role in their formation [10].

The surface of glaciers can be partially or completely covered by a layer of debris (rocks, gravel, ashes, etc.) which affects the ablation rate of the ice underneath and has to be taken into account in models attempting to predict the global melt water discharge of glaciers. If thick enough (typically more than 0.5 cm), a debris cover acts as an insulation layer and reduces the ice ablation rate. On the contrary, a thin layer enhances the ablation rate compared to a bare ice surface [11]. This later effect has been explained by the patchiness of thin layers [12] and by their porosity to air flow [13], although the lower surface albedo of debris can also play a role, especially in the case of ashes [14]. The effect of the presence of a debris layer on the ice ablation rate was well-captured by detailed energy balance models (taking into account the various heat fluxes reaching the surface) [12,15], as well as simpler enhanced temperature index models [16,17] (relying on empirical formulations of the incoming heat fluxes).

On temperate glaciers, two type of structures are related to the presence of debris. On the one hand, glacier tables are rocks supported by an ice foot that forms due to a decrease in the melting rate underneath the stone [18–22]. On the other hand, dirt cones (see Fig. 1) are conical ice structures covered with a thin layer of ashes, grains, or gravel [18,23–27]. Their height typically ranges from 10 cm to 10 m and they form, depending on their size, over the course of a few days to a few weeks in the ablation zone of glaciers, and they can last for a few months. In 1972, a quantitative field study [27] of natural and artificial cones (triggered by the deposition of patches of gravel) showed the existence of an optimum in grain size (1–10 mm) that maximizes the structure formation rate: fine grains are easily washed out by melting water (and possibly rain) while coarse ones do not form a homogeneous protective layer. The author proposed the following qualitative explanation: the thermal protection of the ice by the dirt layer leads, through differential ablation, to the growth of a cone. This causes the debris layer to get thinner as it covers a larger surface area, which reduces its protective effect and ultimately causes the decay of the structure. This process is affected by the evolution of the relative slopes of the ice cone and of the debris layer that modulate the slow granular creep flow, and by the fact that the deformation of the layer reduces its shear strength. The complexity of the overall process did not allow for a quantitative comparison with field observations. In 2001, a theoretical study [8] focused on the initial growth of dirt cones on snow by performing a linear stability analysis. The instability results from the adhesion of grains on

*Corresponding author: nicolas.taberlet@ens-lyon.fr

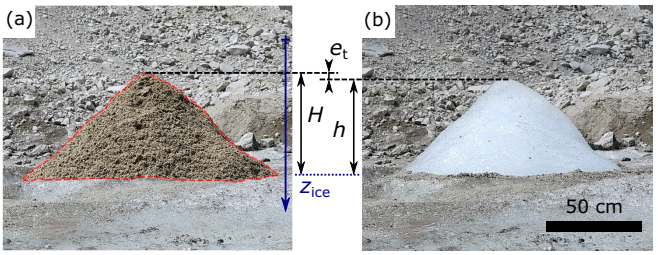

FIG. 1. (a) Dirt cones (red dashed contour) of height H observed at the surface of a temperate glacier (Mer de Glace, Alpes). The vertical position of the ice surface is denoted by z_{ice}. (b) Same structure cleaned of its dirt layer, showing an ice cone of height h. $e_t = H - h$ is the thickness of the dirt layer at the top.

the snow surface, which causes them to accumulate at the top of the cone, locally reducing snow melting. This model cannot be extended to steady-state regimes of ice cones for which the grains do not adhere to the surface and flow along the cone.

In this article, we report a quantitative study of the formation dynamics of dirt cones. We have conducted field observations at Mer de Glace, a temperate glacier in the French Alps, where the formation of dirt cones was monitored over the course of a week. Moreover, we have performed laboratory-scale experiments in simple and well-controlled conditions, and we reproduced the first stage of cone formation. To gain insight on how the deformation of the granular layer is coupled to the evolution of the ice surface, we have developed two-dimensional (2D) numerical simulations taking into account both the quasistatic flow of the granular material forming the dirt layer and the heat transfer across it. Finally, we have developed an analytical model that quantitatively captures the experimental and numerical results and allows a better understanding of the physical processes at play. The article is organized as follows. In Sec. II, we first detail the field observation methods and the laboratory experiments, and we provide a description of the 2D numerical model. The results from the field observations, laboratory experiments, and numerical simulations are then presented in Sec. III. A model of cone formation in the laboratory, for which the heat fluxes received by the ice and debris cover can be considered as proportional to the surface temperature of the receiving body,

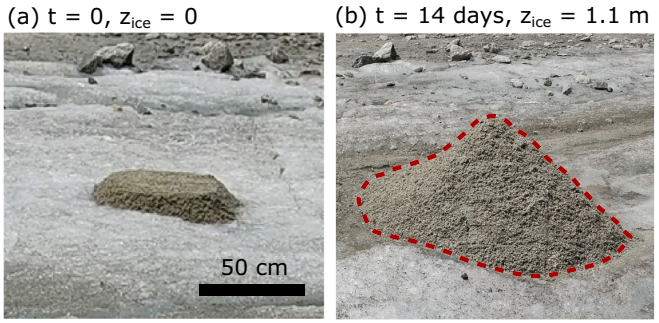

FIG. 2. Formation of a dirt cone. (a) Initial gravel pile (artificially made). (b) Cone formed after 14 days (red contour).

TABLE I. Initial characteristics of the cones studied in the field. V_0 is computed using Eq. (A9) with $\theta_0 = 55^\circ \pm 10^\circ$.

Cone index	R_0 (cm)	e_{t0} (cm)	V_0 (L)
1	24 ± 2	4.5 ± 0.2	7 ± 1
2	26 ± 2	10.0 ± 0.5	19 ± 4
3	12 ± 1	4.9 ± 0.2	1.5 ± 0.3

is described in Sec. IV and accurately predicts the evolution of the dirt-cone observed in the laboratory. This model is then refined to take into account solar radiation and albedo of the ice and of the debris, which successfully reproduces the field observations. Conclusion and perspectives are then presented in Sec. V.

II. MATERIALS AND METHODS

Field observations were performed on the Mer de Glace glacier in the French Alps at an altitude of 2000 m located at 45°54′48.8″ N, 06°56′10.9″ E. To follow the initial formation of a cone, we built three initial piles using small gravel (millimetric grain size) found on the side of the glacier. Grains were compacted into circular shapes of radius R_0 and uniform thickness e_{t0} [see Fig. 2(a), schematics in Fig. 8, and values of the parameters in Table I]. The evolution of the piles was followed using time-lapse images produced by an autonomous solar-powered camera (Enlaps Tikee), positioned on three 1.5-m-long wood rods set into the ice. Pictures (4608 px × 3456 px) were taken every 1 h between 5 a.m. and 10 p.m. between June 7 and June 19, 2019 (see Figs. 1 and 2), until the camera fell on the ice due to the melting around the supporting rods. The residual motion of the device was corrected by tracking two fixed points on the background of each image. The positions of the top of the cone and of the bottom of its left and right sides were then manually pointed out on each image (see video C in the Supplemental Material [28]). The air temperature T_{air} (3 m above ground), solar radiative flux Φ, and wind speed u_{air} were measured at the Requin automatic weather station (AWS) [29] located 600 m higher and 3 km away from the measurement site (see Fig. S-3b-d and Ref. [22] for a discussion on the validity of the assumptions made to compute the local temperature, solar radiative flux, and wind speed).

Small-scale experiments were performed in a laboratory-controlled environment protected from parasite air flow and held at constant temperature $T_{room} = 25.5\,^\circ$C. The granular media consisted of a plastic blast media purchased from Guyson, made of 66–70% urea amino polymer and 33–30% cellulose (density 1.5) with irregular shapes and size lying between 0.84 and 1.20 mm (16/20 mesh size). To prevent cohesion and to minimize the thermal conductivity by avoiding water absorption by the medium, these grains were made hydrophobic using a two-step coating with Rust-Oleum NeverWet multisurface spray. Clear ice blocks (cylinders of diameter 30 cm and height 20 cm) were obtained through unidirectional freezing inside a container thermally isolated on its sides and bottom, and placed inside a −35 °C freezer

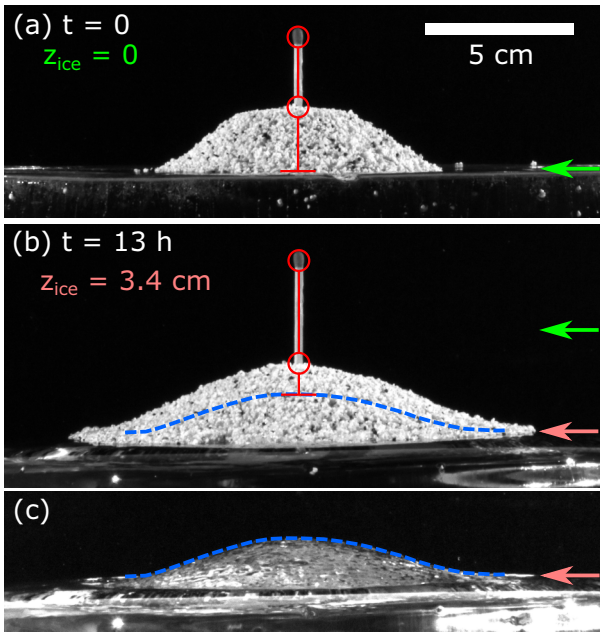

FIG. 3. Formation of an artificial dirt cone in a laboratory-controlled environment. A vertical stick (red) allows us to measure the thickness of the granular layer at the summit of the cone, and to therefore follow the vertical position of the ice surface at the center of the structure (horizontal red line). (a) Initial pile of plastic granular media on a flat ice surface. (b) Cone formed after 13 h. (c) Same cone with its granular cover removed, revealing the surface of the ice (blue line).

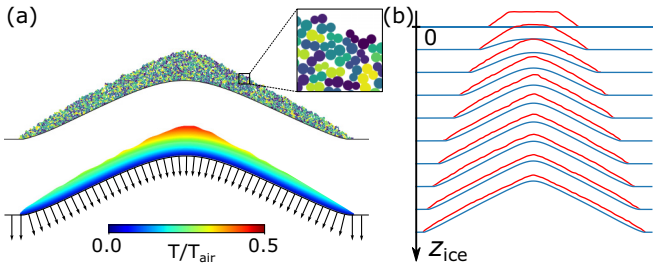

FIG. 4. (a) Principle of the 2D numerical simulations. The granular quasistatic creep flow is determined using a soft-disk discrete element method (top). The temperature distribution in the media is computed using a finite element method (bottom). The displacement of the ice surface v_c is locally proportional to the heat flux (j_c, black arrows). (b) Results of a 2D numerical simulation for an initial piles of thickness e_{t0} equal to the thermal length $\delta = \lambda/h_{eff}$. Only the interfaces [ice/grains (in red) and grains/air (in blue)] are shown.

for 3 days. To ensure a homogeneous temperature $T_{ice} = 0\,^{\circ}$C, the ice block was then left at ambient temperature before the beginning of the experiments.

For each experiment, a flat pile of grains was deposited at the surface of the ice block [see Fig. 3(a)]. The altitude of the ice far from the cone, $z_{ice}(t)$, and the height of its summit, $H(t)$, were monitored. At the center of the pile, a wooden stick was mounted on a small plastic foot lying on the ice surface, allowing us to measure the thickness of the granular layer, $e_t(t)$. It was checked at the end of the experiment that the plastic foot did not penetrate into the ice surface more than 0.5 mm. The pile was illuminated from the sides using two LEDs, and its evolution was followed by taking a picture every 6 min using a D5600 Nikon with a 200 mm lens placed 3.5 m away from the system. Both the 3D field configuration and the 2D numerical configuration (see below) were reproduced: 3D structures were obtained from an initial circular pile of thickness e_0, radius at the bottom, R_0, and angle of repose, $\theta_0 = 36.0^{\circ} \pm 2.5^{\circ}$. Pseudo-2D structures were obtained from initial rectangular piles of half-width R_0 and length $4R_0$. The duration of the experiments was constrained by the melting of the edges of the ice block that limited the maximum lateral extension of the cones.

2D numerical simulations were performed by combining the discrete element method (DEM) to model the granular mechanics with a finite element method to compute the thermal fluxes. The granular media are modeled as an assembly of 2D deformable disks of average radius $\langle r \rangle = 0.25$ mm (with 20% polydispersity), assembled in dimers by adding a constant attractive force within a pair of grains [see Fig. 4(a), top]. The use of dimers is a way to mimic grains of aspect ratio larger than 1, which helps to reach a higher angle of repose [30]. In addition, disks experience gravity and contact forces (normal inelastic repulsion and frictional tangential force). From the sum of all forces and torques acting on each disk, its translational and rotational motion is computed at each time step by classical granular DEM techniques [31]. The values of all numerical parameters are summarized in Table S-I and Table S1. The initial state consists in a trapezoidal pile of thickness e_{t0}, half-width R_0, and angle θ_0 close to the angle of repose of the grains (see Fig. 8) with $e_{t0}/\langle r \rangle \in [40, 120]$ and $R_0/\langle r \rangle \in [80, 240]$. This pile lies on an initially horizontal layer of fixed grains (of size $0.6\langle r \rangle$), representing the first layer of grains glued to the ice surface. At each time step dt, each of these fixed grains (i.e., the local position of the ice surface) is moved downwards by a distance $v_c \times dt$, which varies along the pile as it results from the heat flux within the uneven granular layer. Outside the granular pile, the bare ice surface moves at the ablation velocity v_{ice}, whose value is small enough to lead to a quasistatic granular flow. Below the pile, ice melting is controlled by the heat flux through the granular layer, treated as an effective medium of thermal conductivity λ exchanging heat with air at temperature T_{air} with an effective heat exchange coefficient h_{eff} and in contact with melting ice at temperature T_{ice}. The heat flux j_c delivered to the ice is computed every 5×10^4 time steps by solving the heat equation with the finite element solver FreeFem++ [32] [see Fig. 4(a), bottom]. The ice velocity below the pile is then $v_c = v_{ice} \times j_c/[h_{eff}(T_{air} - T_{ice})]$.

III. RESULTS

In the field and 3D laboratory experiments, initially flat piles of granular media turned into conical structures (see Fig. 2) after the bare ice was ablated by a thickness $z_{ice} \gg e_{t0}$ (far away from the structure). Removing the grain cover showed that these *dirt cones* consist in ice cones covered by a thin layer of grains [see Fig. 1(b)]. The 2D laboratory

TABLE II. Cone angle θ measured from pictures or profiles and angle θ and decompaction factor f used in the model. The $\star$ symbol denotes the parameter kept adjustable in the model.

Context	θ meas.	θ model	f model
Lab	$25^\circ \pm 5^\circ$	23.5° ($\star$)	1
Simulations			
$\mu = 0.6$	$26^\circ \pm 2^\circ$	27° ($\star$)	1
$\mu = 0.3$	$19^\circ \pm 2^\circ$	19° ($\star$)	1
Field	$49^\circ \pm 4^\circ$	49°	1.4 ($\star$)

experiments and numerical simulations displayed a similar behavior: the cross section of the ice surface went from flat to triangular [see Fig. 4(b)]. Both in 2D and 3D, the evolution of the structure can be divided into two stages, clearly visible in the numerical simulation of Fig. 4(b) (see also video B in the Supplemental Material [28]): first, a transient regime which lasts until the flat region at the center of the pile disappears and the shape becomes conical (or triangular), then a stable regime in which the cone keeps growing while keeping a constant slope. It is visible in the film that the grain flow is not limited to avalanches at the surface but also takes place in the bulk of the cover layer. The quantities used in the following to quantitatively characterize the structure evolution are shown in Fig. 1: h denotes the height of the ice dome, e_t is the thickness of the grain layer at the top, and $H = h + e_t$ is the total height. In the cone regime, the slope of the ice cone and that of the dirt cone differ by only a few degrees [27]: in the following, this difference will be neglected and a unique value θ is used. This value strongly depends on the nature of the granular medium: the measured values are displayed in Table II and range from 19° for dry, low friction grains in the simulation, to 49° for wet gravel in the field. Let us note that these angles are systematically lower than the repose angle of the grains by 5°–10°.

In our field observations, only the evolution of the total height H with time (and therefore with $z_{ice} = v_{ice}\, t$) was accessible and is plotted in Fig. 5. In numerical simulations and laboratory experiments, all quantities h, e_t, and H could be monitored: Figs. 6 and 7 show $H(z_{ice})$ and $e_t(h)$ for different initial pile shapes. All these data qualitatively display the same behavior: first, the growth rate of the cone height dH/dz_{ice} is maximum during the transient regime. For the largest initial radius, this rate keeps a constant value for a little while, meaning that the height first evolves linearly. This is particularly visible on the field data. In this first stage, in the laboratory and in the simulations, the thickness at the summit, e_t, diminishes only slightly ($\lessapprox$10%). Once the cone regime is reached, the growth rate of the cone strongly decays, while the granular cover on top quickly thins down. At long times (i.e., for $v_{ice}\, t \gg R_0$), we observe in the field experiments (red markers in Fig. 5) and in the simulations [blue line in Fig. 7(b)] that the growth rate tends to zero. This corresponds to a cone that dynamically keeps the same shape and size while its internal ice is melting at the same rate as the bare ice surface. In the laboratory experiments, this last regime is not accessible due to the limited size of the ice blocks.

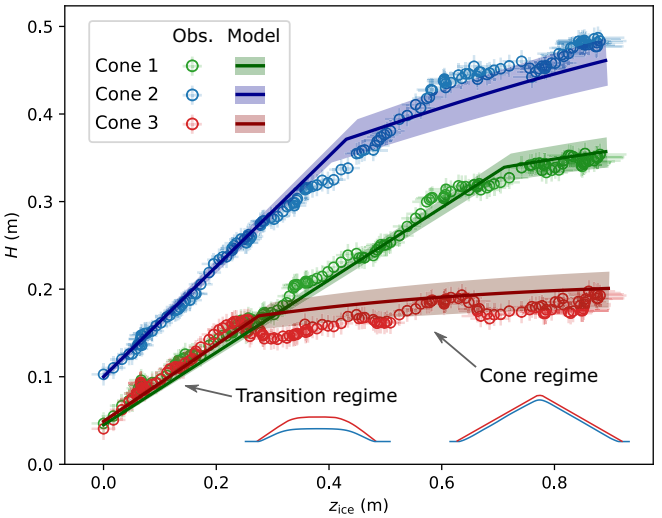

FIG. 5. Cone formation dynamics on the Mer de Glace for the three gravel piles described in Table I. The total cone height H is shown as a function of the total ice ablated thickness z_{ice} (markers). The model is plotted by a solid line for each initial state (e_{t0}, V_0, the shaded area corresponds to the uncertainty on these parameters) with adjustable parameter $f = 1.4$.

IV. MODELING AND DISCUSSION

A. Cone formation in the laboratory and in simulations

In the following, we develop a simple model of the formation of a cone from an initial flat pile of grains (see Fig. 8). We first concentrate on the simpler case in which all the heat fluxes coming from the environment can be considered as proportional to the surface temperature of the receiving body. As discussed below, this applies well to our laboratory experiments and was implemented in the numerical simulations presented in this work. On a natural glacier, however, the process is also affected by direct solar radiation, and this case will be treated in the next subsection.

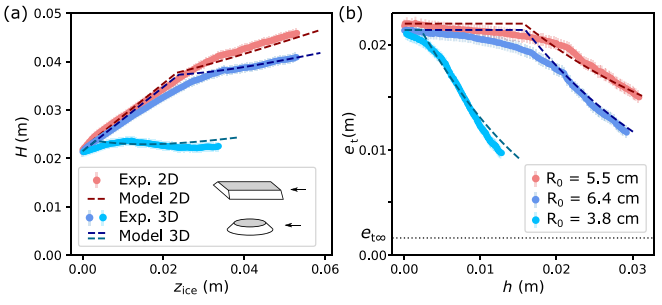

FIG. 6. (a), (b) Cone formation in the laboratory-controlled environment (markers) in a 2D (red) and 3D (blue) configuration. The total cone height H is shown as a function of the ablated ice thickness z_{ice} (a) and the granular thickness as the top of the cone e_t as a function of its height h (b). The model (see Sec. IV) is plotted as a dashed line for the corresponding geometry (2D/3D) and for each initial state (e_{t0}, R_0) with adjustable parameter $\theta = 23.5^\circ$.

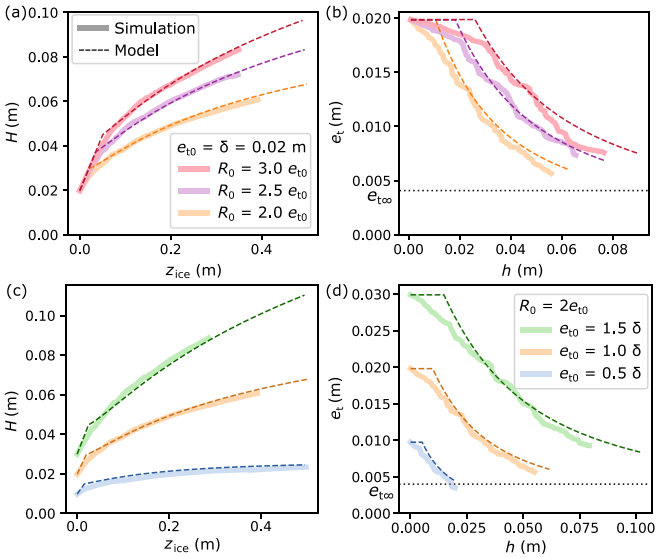

FIG. 7. Results of 2D numerical simulations (solid lines) for $\mu = 0.6$. The quantities plotted are the same as in Fig. 6. The model is plotted as a dashed line for each initial state (e_{t0}, R_0) with adjustable parameter $\theta = 27^\circ$.

1. Ice melting

The ice surface away from the granular pile gets lower due to melting under the effect of a positive net incoming heat flux $Q_{\text{env.}\to\text{ice}}$ coming from the environment. Its vertical position $z_{\text{ice}}(t)$ can be expressed, assuming that the melting process is instantaneous, as $z_{\text{ice}}(t) - z_{\text{ice}}(0) = \mathcal{L}_{\text{fus}} \int_0^t Q_{\text{env.}\to\text{ice}}(t)dt$, where $\mathcal{L}_{\text{fus}} = 303\ \text{MJ m}^{-3}$ is the volumetric enthalpy of fusion for ice. In a laboratory-controlled environment, the incoming heat flux has two main origins [21]: the net infrared radiation coming from the enclosure walls (at temperature T_{room}) and the natural convection of air (also at temperature T_{room}). Since $T_{\text{room}} - T_{\text{ice}} \ll T_{\text{ice}}$, its expression can be linearized as

$$Q_{\text{env.}\to\text{ice}} = h_{\text{eff}}(T_{\text{room}} - T_{\text{ice}}), \tag{1}$$

where $h_{\text{eff}} = 8 \pm 2\ \text{W K}^{-1}\ \text{m}^{-2}$ is an effective heat exchange coefficient that was measured by monitoring the melting of an ice block (see the Supplemental Material [28]).

2. Early stage of the transition regime

At the very beginning of the process, the structure consists in a flat pile of grains that acts as an insulating cover: the dirt

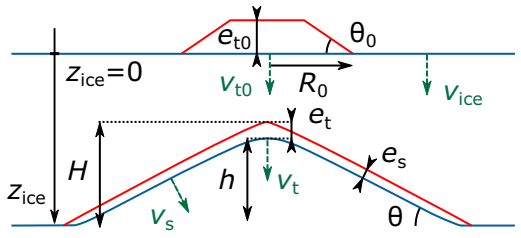

FIG. 8. Schematics of an initial pile of grains (top) and of the cone forming when the ice surface melts (bottom). The blue curve corresponds to the ice surface and the red curve to the top of the granular cover.

surface being warmer than the ice, it receives less heat from the environment, and therefore $Q_{\text{dirt}\to\text{ice}} < Q_{\text{env.}\to\text{ice}}$.

As long as $R_0 \gg e_{t0}$, the process at the center of the pile can be considered as one-dimensional (1D), which leads to a simple analytical formulation. Assuming that the effective heat exchange coefficient h_{eff} is the same for the dirt and the ice surfaces, the ratio of melting velocity between covered and bare ice is, at $t = 0$,

$$\frac{v_{t0}}{v_{\text{ice}}} = \frac{Q_{\text{dirt}\to\text{ice}}}{Q_{\text{env.}\to\text{ice}}} = \frac{1}{1 + e_{t0}/\delta}, \tag{2}$$

where $\delta = \lambda/h_{\text{eff}}$ is a thermal characteristic length and λ is the effective thermal conductivity of the dirt layer ($\text{Bi} = e_{t0}/\delta$ is the Biot number). This differential ablation of ice leads to the growth of an ice foot under the dirt pile (in the referential of the bare ice surface) at a rate

$$\frac{dh}{dz_{\text{ice}}} = 1 - \frac{v_t}{v_{\text{ice}}}, \tag{3}$$

where v_t is the vertical melting velocity below the center of the structure. In the early stages, the top of the pile remains flat: there is no driving force leading the grains to move laterally and we can assume that $e_t \approx e_{t0}$. Combining Eqs. (2) and (3) leads to

$$H = h + e_t = \frac{\text{Bi}}{1 + \text{Bi}} \times z_{\text{ice}}. \tag{4}$$

Using the measured value of the thermal length for the plastic grains $\delta = 10.8 \pm 0.3$ mm (measured in an independent experiment; see Fig. S-1), this prediction is plotted (with no adjustable parameter) in Fig. 6(a) as dashed straight lines. For the wider piles ($R_0 = 5.5$ and 6.4 cm), for which the 1D approximation is most valid, the prediction fits the observations for $0 < z_{\text{ice}} < 2$ cm. For the smallest pile ($R_0 = 3.8$ cm, light blue), the model overestimates the initial growth rate, and the linear growth regime is not observed. But even large piles eventually reach a point where the assumptions made above are no longer valid: the grains at the center are affected by the lateral flow induced by the deformation of the sides. As a consequence, e_t decreases and the thermal problem is not 1D anymore. This induces a complex dynamics that ultimately leads to the formation of a conic structure and which is only described qualitatively here. Differential ablation deforms the ice surface at the periphery of the pile, which induces a quasistatic flow in the grain cover whose free surface adopts a slope θ_{grains}. The flow modifies the cover thickness and couples back with the deformation of the ice surface, which takes a slope $\theta_{\text{ice}} < \theta_{\text{grains}}$ [see Fig. 4(b)]. As the cover is thinner on the outside, the ice melts faster on the outside, causing the two angles to converge to the same value θ. The conic shape is obtained when the deformation reaches the center. The fact that the final structure is a cone rather than a smooth dome results from the fact that as the structure grows, its typical dimensions (radius and height) both exceed the thermal length δ ($\approx$11 mm), which controls the scale over which the ice profile can vary. In the laboratory, due to the experimental constraints on the size of the ice block, δ was made as small as possible by using rather insulating grains, yet the ratio H/δ is still significantly smaller than in the simulations or on the field. This explains (alongside with the difference in θ) the

different shape of the ice cones obtained in the laboratory [Fig. 3(c): smooth with low angle], in simulations [Fig. 4(b): conic with low angle], and in the field (Fig. 1: conic with large angle).

3. Cone regime

In the following, we focus on a structure that has already reached the cone regime (i.e., $e_t, e_s \ll H$). Let us assume that the approximations $e_t \approx e_{t0}$ and $v_t \approx v_{t0}$ [given by Eq. (2)] are valid throughout the whole transition phrase: the cone regime is then reached for a total ablation $z_{ice} = z_1 = h_1/(1 - v_{t0}/v_{ice})$, where h_1 is the initial height of the cone at the end of the transient regime. Considering that the total volume $\mathcal{V}$ of the granular cover is conserved, h_1 can be expressed (in 2D or 3D) as a function of initial parameters θ_0, R_0, and e_{t0} [see Eqs. (A10) and (A11) in the Appendix].

To develop a simple analytical model of the later stage, the following assumptions are made:

(i) The thermal problem can be considered 1D for the dirt on the sides of the cone: $v_s/v_{ice} = 1/(1 + e_s/\delta)$. This is valid far away from the transition regime, when $e_s \ll h/\tan\theta$.

(ii) The angle of the cone, as well as the shape of the top of the ice cone, are stationary. This is supported by the numerical simulations [see Fig. 4(b)]. From this, we can relate the melting velocity at the summit to that on the side of the cone: $v_t = v_s/\cos\theta$.

(iii) The ratio $A = e_s/e_t$ is a constant. Although not obvious (since this ratio results from the granular flow and the melting on top of the cone), this assumption is supported by the numerical simulations where A is observed to be constant and independent of the cone angle (for $\theta = 19^\circ$ and 26°): $A = 0.6 \pm 0.1$. In laboratory experiments and in the field A can only be measured at the end of the evolution, but this final value is equal to the numerical value and independent of the initial shape of the pile (see Fig. S-5).

From these assumptions, the growth rate of the cone height can be expressed as a function of $e_t(h)$:

$$\frac{dh}{dz_{ice}} = 1 - \frac{1}{\cos\theta} \times \frac{1}{1 + Ae_t(h)/\delta}. \tag{5}$$

The state at the end of the transient regime is defined by $z_{ice} = z_1$, $h(z_1) = h_1$, and $e_t(h_1) = e_{t0}$. Through volume conservation, we express the quantity e_t both in the 2D and 3D cases (see the Appendix). Finally we solve Eq. (5) numerically with θ_0, R_0, e_{t0}, A, and δ as input parameters. We keep θ as the only adjustable parameter, due to the high sensibility of the model to this quantity. Furthermore, the value of θ results from a complex feedback between the evolution of the ice surface and the creep flow in the granular cover, which prevents us from predicting a simple *a priori* estimate.

The best-fitting resulting evolution is shown for laboratory experiments in Fig. 6 ($\theta = 23.5^\circ$) and for numerical simulations in Fig. 7 ($\theta = 27^\circ$ and $\mu = 0.6$) (see the Supplemental Material [28] for results concerning $\mu = 0.3$). The values of the adjustable parameter θ (see Table II) are within the range of the values that were measured independently.

The good agreement in the $e_t(h)$ plots of Figs. 6(b) (in 2D and 3D) and 7(b)–7(d) (in 2D) supports in retrospect the assumption of volume conservation in the cone regime. This also shows that the difference in the cone formation dynamics between the 2D and 3D cases is mainly related to the volume conservation. This justifies the relevance of the 2D simulations in testing the other assumptions (i)–(iii) of the model, related to mechanical and thermal processes. Our description of the transition regime (constant e_t) is too simplistic: since e_t shows a perceptible decrease, the model overestimates the growth rate dh/dz_{ice} but underestimates z_1. Remarkably, these errors compensate, which leads to a good agreement between the prediction and the observed evolution $H(z_{ice})$ in the cone regime.

4. Steady state

At long times, Eq. (5) predicts the existence of a steady state in which $e_{t,\infty} = \delta(1/\cos\theta - 1)/A$. This value is independent of the initial conditions (which is not the case of the steady-state height and radius of the cone) and is represented in Figs. 6(b), 7(b), and 7(d) using dotted horizontal lines. One can see that only the numerical simulation with the smallest initial thickness approaches its final state. In the laboratory experiment, it was not possible to reach the steady state since, given the low cone angle, the finite size of the ice block was quickly limiting the maximum value of z_{ice}.

B. Natural cone formation on a glacier

The formation of natural dirt cones occurring at the surface of a glacier is slightly more complex than the process taking place in the well-controlled laboratory conditions, mainly because the heat flux coming from the environment cannot simply be described using an effective heat exchange coefficient. Indeed, in the previous model the heat flux received by the ice and dirt surfaces is governed by their temperatures. This is not the case for the solar heat flux, which plays a crucial role in the field. In the following, we show that the previous model can be adapted to these conditions with only minor modifications.

1. Ice melting

In the field, the main heat source is direct solar irradiation. For our field data, it represented 60% of the total incoming flux, the rest coming from the turbulent fluxes (convection and sublimation or condensation due to the wind), whereas the net infrared radiation was almost null (but negative) [22]. While it is possible to model in detail these physical processes, another approach classically used in glaciology is to rely on an empirical relation known as an enhanced temperature index model [16,17,33]. Let us assume that all contributions other than net solar radiation can be described by an empirical term proportional to the difference between air and surface temperature:

$$Q_{env.\to ice} = (1 - \alpha_{ice})\Phi(t) + h_{eff}(\langle T_{air}\rangle - T_{ice}), \tag{6}$$

where α_{ice} is the ice surface albedo, $\Phi(t)$ is the incoming solar radiation, $\langle T_{air}\rangle$ is the mean air temperature, T_{ice}=273 K is the melting ice temperature, and h_{eff} is an empirical coefficient that has the dimension of an effective heat exchange coefficient. The data of $z_{ice}(t)$ are shown in the Supplemental Material [28] (see Fig. S-3) and are used to

determine the values of α_{ice} and h_{eff} by adjusting the model of Eq. (6). A good overall agreement, given the simplicity of the model, is obtained with $\alpha_{\text{ice}} = 0.32 \pm 0.02$ and $h_{\text{eff}} = 14.8 \pm 0.5$ W K^{-1} m^{-2}, which is consistent with common values found in the literature for alpine glaciers [34,35]. As detailed in the Supplemental Material [28], h_{eff} depends on the mean wind speed on the glacier, which was constantly high in the period of interest.

2. Early stage of the transition regime

The heat flux received by the dirt layer can be split into two parts: one that depends on its surface temperature (less than what is received by bare ice if the dirt is warmer than T_{ice}) and one received from the sun, which depends on the dirt albedo α_{dirt}. The calculation leading to Eq. (2) can be adapted for the daily averaged ratio of melt velocities in the presence of solar radiation:

$$\left\langle \frac{v_{t0}}{v_{\text{ice}}} \right\rangle = \frac{1}{1+\text{Bi}} \times \frac{1+(1-\alpha_{\text{dirt}})\langle\tilde{\Phi}\rangle}{1+(1-\alpha_{\text{ice}})\langle\tilde{\Phi}\rangle}, \tag{7}$$

where $\langle\tilde{\Phi}\rangle = \langle\Phi(t)\rangle/[h_{\text{eff}}(\langle T_{\text{air}}\rangle - T_{\text{ice}})] \approx 2.4$ is a dimensionless number accounting for the effect of solar radiation. This means that the albedo difference has only a correcting effect, and that the insulating effect acts on the total heat flux. This can be interpreted as follows: the solar incoming flux induces a strong thermal gradient across the dirt layer (whose bottom stays at T_{ice}). This, in return, reduces (or even changes the sign, if the surface temperature is higher than T_{air}) the other heat fluxes (wind induced, infrared, etc), ultimately reducing the heat flux received by the covered ice.

The effective thermal conductivity of wet gravel collected on the Mer de Glace was measured in the laboratory and found to be $\lambda_{\text{Gravel}} = 0.73 \pm 0.05$ W m^{-1} K^{-1} (see the Supplementary Material [28]). Given the mean effective heat exchange coefficient during the studied time period, this corresponds to a thermal length $\delta = 4.9 \pm 0.4$ cm. On the field data of Fig. 5, an initial linear regime is clearly visible for $z_{\text{ice}} < 0.2$ m, with a higher slope (corresponding to a more insulating behavior) for the thickest pile. Assuming that $e_t \approx e_{t0}$, Eq. (7) can be used to extract the last unknown parameter α_{dirt} from these data. The best-fitting value is $\alpha_{\text{dirt}} = 0.20 \pm 0.05$ (see Fig. S-1), which is compatible with values commonly used for gravel [36] or granite rock [22,37].

3. Cone regime

We assume that conditions (i)–(iii) of the previous model (Sec. IV A) remain valid in the field. The hypothesis of volume conservation, however, needs to be adapted. Indeed, due to the cohesive nature of wet gravel and to the fact that the initial piles were compacted by hand, a decompaction can occur during the transition regime: the dirt volume V in the cone regime is therefore larger than the initial volume V_0. We characterize this process by the parameter $f = V/V_0$. By comparing its dimensions in the initial and final states, we measured $f = 1.4 \pm 0.3$ for the cone shown in Fig. 1 (see the Supplemental Material [28]). We also noticed that the dirt covering natural cones on the glacier could easily be compacted by hand by ≈20–40%. In the following, we keep the assumption that the dirt volume is conserved throughout the cone regime, with the value $V = fV_0$. The melting velocity v_s on the side of the cone also has to be adapted in order to take into account the presence of solar radiation and the fact that the corresponding heat flux reaches the sides of the cone with an angle (averaged over a day and compared to a flat surface) which reduces the flux by a factor $\cos\theta$. This leads to

$$\frac{dh}{dz_{\text{ice}}} = 1 - \frac{1}{\cos\theta}\frac{1}{1+Ae_t(h)/\delta}\frac{1+(1-\alpha_{\text{dirt}})\langle\tilde{\Phi}\rangle\cos\theta}{1+(1-\alpha_{\text{ice}})\langle\tilde{\Phi}\rangle}. \tag{8}$$

By following the same steps as in Sec. IV A, $H(z_{\text{ice}})$ can be computed for each cone, as shown by solid lines in Fig. 5. The computation uses the parameters A, h_{eff}, α_{ice}, α_{dirt}, λ_{Gravel}, $\langle\tilde{\Phi}\rangle$, and θ given previously, and e_{t0} and V_0 are given for each cone in Table I. The only adjustable parameter here is the decompaction factor f, and the best-fitting value was $f = 1.4$. The main source of uncertainty on the model prediction, shown using a shaded area in Fig. 5, is the inaccuracy on V_0 (15–20%).

The beginning of the cone regime is well predicted for the thinnest cones (1 and 3) but is a bit premature for cone 2, which leads to a systematic underestimation of H. In the cone regime, the growth rate of the height is very well predicted for all three cases. Cone 2 starts with a dirt thickness about three times higher than the fixed point of Eq. (8): $e_{t,\infty} \approx 3.4$ cm, which leads to a rapid growth in the cone regime as a lot of dirt will flow before the protective layer gets thin enough to reach the stationary regime. The model predicts a final height $H_\infty \approx 57$ cm reached within 5% at $z_{\text{ice}} \approx 2.2$ m. Cones 1 and 3, however, start with a dirt thickness $e_{t,0}$, close to $e_{t,\infty}$, which explains why they do not grow much in the cone regime, as they have already almost reached their maximum height.

4. Steady state

As the cone height grows causing the dirt to flow, the cover gets thinner and less insulating. At some point $e_t = e_{t\infty}$, which corresponds to $v_t = v_{\text{ice}}$, and a steady state is reached. This final thickness is independent of the initial state and is fixed by the properties of the cover layer (thermal conductivity and mechanical properties) as well as the characteristics of the incoming heat (mainly h_{eff} and to a lesser extent $\langle\tilde{\Phi}\rangle$ and the ice and dirt albedo). It is worth noting that the final thickness, which controls the dynamics, can vary substantially over time on a glacier as h_{eff} depends on the average wind speed. The growth rate of a dirt cone can thus keep evolving even long after its formation. For example, a cone that forms and reaches a stationary state during a calm period (low h_{eff} and high δ) will start growing again during a windy period (high h_{eff} and low δ).

V. CONCLUSION AND PERSPECTIVES

In this article, we described small-scale experiments reproducing dirt cone formation in a well-controlled laboratory environment as well as time-resolved observations of the formation of three cones on the Mer de Glace. Dirt cone formation was also studied through 2D numerical simulations taking into account both the grain mechanics and the thermal heat exchanges that are able to reproduce well the

cone formation process. A simple model was developed and led to a quantitative agreement with the laboratory and field observation as well as the simulations. This combination of approaches allowed us to gain insight into the physical mechanisms governing this structure formation.

A dirt layer lying at the surface of a glacier acts as an insulation cover that reduces the ice melting under it. The differential ablation causes the ice surface to deform, which induces a quasistatic flow of the dirt, starting from the edge of the pile. The structure acquires its conic shape when the deformation reaches the summit. The angle of the cone is determined by the mechanical properties of the grains (friction, cohesion) but does not correspond to a repose angle and is probably dependent on the history of stress distribution during the cone formation. As long as the dirt layer covering the cone is thick enough to reduce ice melting, the cone height will grow causing the dirt to creep along the sides and get thinner and less insulating. Finally, a stationary state is reached in which the insulating dirt cover exactly compensates for the fact that the structure received heat on a higher surface or with a lower albedo. In the model we developed, this final state is stable, which can explain the month-long lifetime of dirt cones on glaciers (while they typically form within a week).

Our field observations along with the modeling open the possibility to use dirt cones as a proxy to estimate environmental parameters such as the heat exchange coefficient of the glacier ablation rate. On glaciers, the lifetime of dirt cones is limited (to a few months) and the process by which this happens remains unexplained. It may be related to the progressive degradation of the dirt layer under the effect of rain or melt water, but clearly it deserves further attention. Another question that remains open is the formation of a "cone forest" observed on glaciers, consisting of several cones of various height, all in contact with each other. They clearly emerge from an initial large patch of dirt, but whether individual cones appear due to thickness inhomogeneity or from a more puzzling physical instability remains to be clarified.

ACKNOWLEDGMENTS

The authors are grateful to Marine Vicet, Jérémy Vessaire, and Thierry Dauxois for fruitful discussions, to the Fédération de Recherche Marie André Ampère, and to the Laboratoire de Physique at the ENS de Lyon for financial support.

APPENDIX: VOLUME CONSERVATION

In the model developed in the main text, one important assumption is the volume conservation of the granular cover. In the following, we detail the corresponding calculation.

In the cone regime, the dirt cone is assumed to have a constant thickness $e_s = Ae_t$. In 2D, the dirt layer has a length $\approx (h + e_t/2)/\sin\theta$ on each side. The volume per unit depth can thus be approximated as

$$\mathcal{V}_{2D} = \frac{A}{\sin\theta}(2h + e_t)e_t. \tag{A1}$$

This quantity is assumed to be constant, $d\mathcal{V}_{2D} = 0$, leading to the following differential equation:

$$1 + \frac{h}{e_t} + \frac{dh}{de_t} = 0 \tag{A2}$$

whose solution is

$$h(e_t) = \frac{e_{t0}}{e_t}\left(h_1 + \frac{e_{t0}}{2}\right) - \frac{e_t}{2} \tag{A3}$$

which can be inverted in

$$e_{t\,2D}(h) = \sqrt{h^2 + 2e_{t0}\left(h_1 + \frac{e_{t0}}{2}\right)} - h. \tag{A4}$$

In 3D, the same approximation leads to a volume

$$\mathcal{V}_{3D} = \frac{\pi A}{\sin\theta\tan\theta}e_t\left(h + \frac{e_t}{2}\right)^2. \tag{A5}$$

The condition $d\mathcal{V}_{3D} = 0$ corresponds to

$$\frac{3}{2} + \frac{h}{e_t} + 2\frac{dh}{de_t} = 0 \tag{A6}$$

whose solution is

$$h(e_t) = \frac{h_1\sqrt{e_{t0}} + e_{t0}^{3/2}/2}{\sqrt{e_t}} - \frac{e_t}{2}. \tag{A7}$$

The expression of $e_{t\,3D}(h)$ is then obtained by keeping the only real solution of the cubic equation with unknown $x = \sqrt{e_t}$.

The volume of the initial pile in 2D and 3D is

$$\mathcal{V}_{2D\,0} = \left(R_0 - \frac{e_{t0}}{\tan\theta_0}\right)e_{t0}, \tag{A8}$$

$$\mathcal{V}_{3D\,0} = \frac{\pi}{3}\tan\theta_0\left[R_0^3 - \left(R_0 - \frac{e_{t0}}{\tan\theta_0}\right)^3\right]. \tag{A9}$$

If the volume is assumed to be conserved from the initial flat pile state to the cone regime, the parameter $h_1 = h(e_{t0})$ can be expressed as

$$h_{2D\,1} = \left(R_0 - \frac{e_{t0}}{2\tan\theta_0}\right)\frac{\sin\theta}{A} - \frac{e_{t0}}{2}, \tag{A10}$$

$$h_{3D\,1} = \sqrt{\frac{\mathcal{V}_0\sin\theta\tan\theta}{A\pi e_{t0}}} - \frac{e_{t0}}{2}. \tag{A11}$$

[1] R. Bintanja, C. H. Reijmer, and S. J. M. H. Hulscher, J. Glaciol. **47**, 387 (2001).
[2] N. Mangold, Geomorphology **126**, 1 (2011).
[3] V. Bergeron, C. Berger, and M. D. Betterton, Phys. Rev. Lett. **96**, 098502 (2006).
[4] P. Claudin, H. Jarry, G. Vignoles, M. Plapp, and B. Andreotti, Phys. Rev. E **92**, 033015 (2015).
[5] N. Taberlet and N. Plihon, Proc. Natl. Acad. Sci. USA **118**, e2109107118 (2021).
[6] M. Bushuk, D. M. Holland, T. P. Stanton, A. Stern, and C. Gray, J. Fluid Mech. **873**, 942 (2019).
[7] S. Weady, J. Tong, A. Zidovska, and L. Ristroph, Phys. Rev. Lett. **128**, 044502 (2022).
[8] M. D. Betterton, Phys. Rev. E **63**, 056129 (2001).

[9] K. A. Mitchell and T. Tiedje, J. Geophys. Res. **115**, F04039 (2010).
[10] J. J. Rhodes, R. L. Armstrong, and S. G. Warren, J. Glaciol. **33**, 135 (1987).
[11] G. Östrem, Geogr. Annal. **41**, 228 (1959).
[12] T. D. Reid and B. W. Brock, J. Glaciol. **56**, 903 (2010).
[13] G. W. Evatt, I. D. Abrahams, M. Heil, C. Mayer, J. Kingslake, S. L. Mitchell, A. C. Fowler, and C. D. Clark, J. Glaciol. **61**, 825 (2015).
[14] A. Rivera, F. Bown, D. Carrión, and P. Zenteno, Environ. Res. Lett. **7**, 014036 (2012).
[15] E. Collier, L. Nicholson, B. Brock, F. Maussion, R. Essery, and A. Bush, The Cryosphere **8**, 1429 (2014).
[16] M. Carenzo, F. Pellicciotti, J. Mabillard, T. Reid, and B. W. Brock, Adv. Water Resour. **94**, 457 (2016).
[17] R. Möller, M. Moeller, P. A. Kukla, and C. Schneider, J. Glaciol. **62**, 933 (2016).
[18] L. Agassiz, *Études sur les Glaciers* (Gent & Gassman, Neuchâtel, 1840)
[19] E. Bouillette, L'Astronomie **47**, 201 (1933).
[20] E. Bouillette, L'Astronomie **48**, 89 (1934).
[21] M. Hénot, N. Plihon, and N. Taberlet, Phys. Rev. Lett. **127**, 108501 (2021).
[22] M. Hénot, V. J. Langlois, J. Vessaire, N. Plihon, and N. Taberlet, The Cryosphere **16**, 2617 (2022).
[23] C. Swithinbank, J. Glaciol. **1**, 461 (1950).
[24] J. W. Wilson, J. Glaciol. **2**, 281 (1953).
[25] L. O. Krenek, J. Glaciol. **3**, 312 (1958).
[26] I. B. Campbell and G. G. C. Claridge, New Zealand J. Geol. Geophys. **18**, 349 (1975).
[27] D. J. Drewry, J. Glaciol. **11**, 431 (1972).
[28] See Supplemental Material at http://link.aps.org/supplemental/10.1103/PhysRevE.107.034905 for movies of laboratory experiments, numerical simulations and field observations and for additional information about the numerical simulations and the evaluation of parameters in the laboratory and on the field.
[29] D. F. Nadeau, W. Brutsaert, M. Parlange, E. Bou-Zeid, G. Barrenetxea, O. Couach, M.-O. Boldi, J. S. Selker, and M. Vetterli, Environ. Fluid Mech. **9**, 635 (2009).
[30] Z. Zhou, R. Zou, D. Pinson, and A. Yu, Granular Matter **16**, 695 (2014).
[31] T. Pöschel and T. Schwager, *Computational Granular Dynamics: Models and Algorithms* (Springer-Verlag, Berlin, 2005).
[32] F. Hecht, J. Numer. Math. **20**, 251 (2012).
[33] F. Pellicciotti, B. Brock, U. Strasser, P. Burlando, M. Funk, and J. Corripio, J. Glaciol. **51**, 573 (2005).
[34] B. W. Brock, I. C. Willis, and M. J. Sharp, J. Glaciol. **46**, 675 (2000).
[35] C. Vincent and D. Six, Ann. Glaciol. **54**, 11 (2013).
[36] J. I. Peltoniemi, J. Piironen, J. Näränen, J. Suomalainen, R. Kuittinen, L. Markelin, and E. Honkavaara, ISPRS J. Photogr. Remote Sens. **62**, 434 (2007).
[37] R. D. Watson, Remote Sensing Environ. **2**, 95 (1971).